SUPPLEMENTARY INFORMATION

Discovery of the first-in-class dual histone deacetylase-proteasome inhibitor

Sanil Bhatia,[‡,1] Viktoria Krieger,[‡,2] Michael Groll,[3] Jeremy D. Osko,[4] Nina Reßing,[5] Heinz Ahlert,[1] Arndt Borkhardt,[1] Thomas Kurz,[2] David W. Christianson,[4] Julia Hauer[,§,1] and Finn K. Hansen*[,§,5]*

[1]Department of Pediatric Oncology, Hematology and Clinical Immunology, Medical Faculty, Heinrich Heine University Düsseldorf, Moorenstr. 5, 40225 Düsseldorf, Germany

[2]Institute for Pharmaceutical and Medicinal Chemistry, Heinrich Heine University Düsseldorf, Universitätsstrasse 1, 40225 Düsseldorf, Germany

[3]Center for Integrated Protein Science at the Department Chemie, Lehrstuhl für Biochemie, Technische Universität München, Lichtenbergstrasse 4, 85747 Garching, Germany

[4]Roy and Diana Vagelos Laboratories, Department of Chemistry, University of Pennsylvania, 231 South 34th Street, Philadelphia, PA 19104-6323, United States

[5]Pharmaceutical/Medicinal Chemistry, Institute of Pharmacy, Medical Faculty, Leipzig University, Brüderstr. 34, 04103 Leipzig, Germany

‡ These authors contributed equally to this work as first authors.

§ These authors contributed equally to this work as senior authors.

Corresponding authors:

Finn K. Hansen, Pharmaceutical/Medicinal Chemistry, Institute of Pharmacy, Medical Faculty, Leipzig University, Brüderstr. 34, 04103 Leipzig, Germany, Tel: +49 341 97 36801, Fax: +49 341 97 36889, E-mail: finn.hansen@medizin.uni-leipzig.de

Julia Hauer, Department of Pediatric Oncology, Hematology and Clinical Immunology, Heinrich Heine University Düsseldorf, Medical Faculty, Moorenstr. 5, 40225 Duesseldorf, Germany, Tel: +49 211 81 17680; Fax: +49 211 81 16206; e-mail: Julia.Hauer@med.uni-duesseldorf.de

Table of Contents

1. Supplemental Figures and Tables S3
2. Chemistry S12
3. X-ray crystallography S13
4. ^{1}H-, ^{13}C-NMR spectra and HPLC chromatogram S15
5. References S21

1. Supplemental Figures and Tables

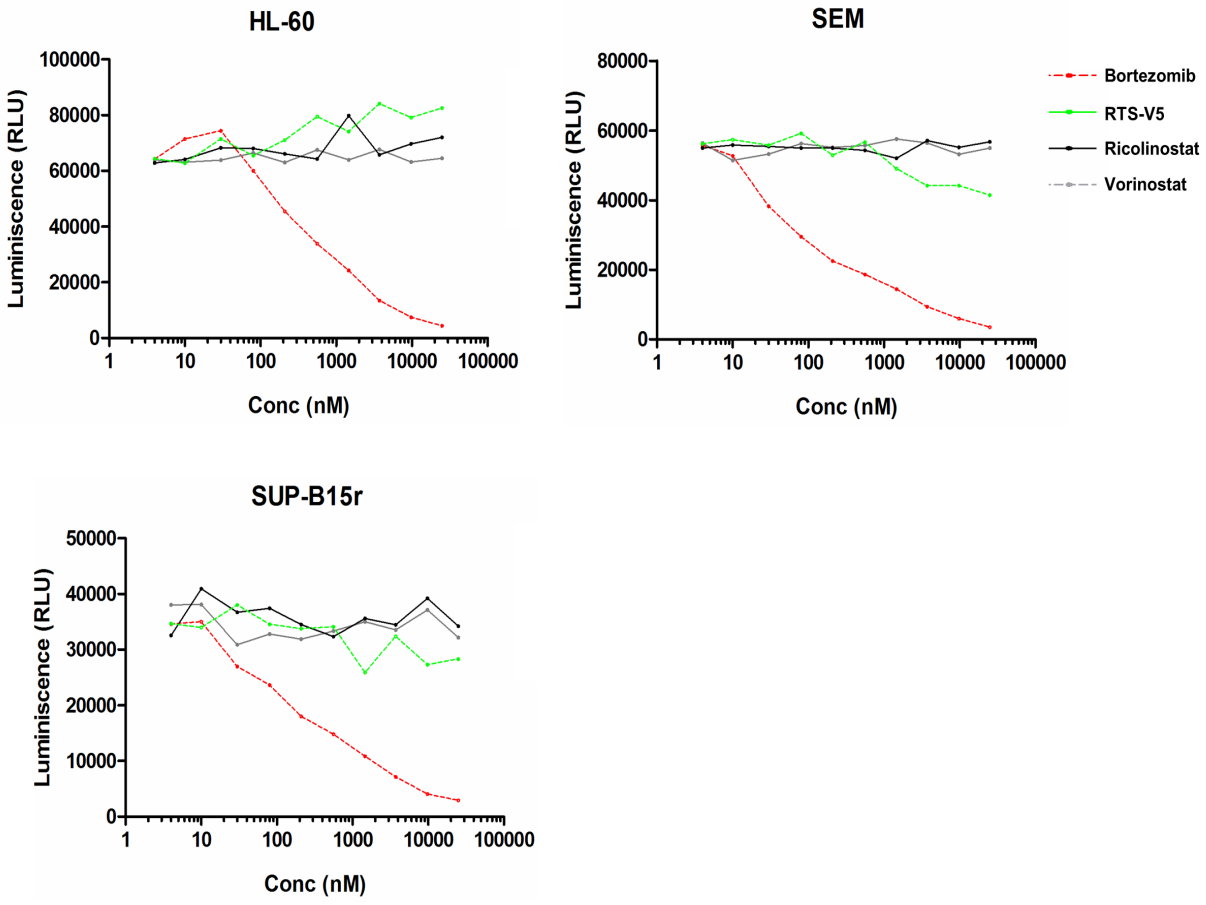

Figure S1a. Proteasome inhibition assay (Trypsin-Like activity). HL-60, SEM, and SUP-B15r cells were treated for 2 h with bortezomib, vorinostat, ricolinostat, and RTS-V5 at concentrations ranging from 4 nM-25 µM. The proteasomal activity was measured after 2 h using a Cell-Based Proteasome-Glo Trypsin-Like assay by taking Z-LRR-aminoluciferin (Z-leucine-arginine-arginine-aminoluciferin) as a substrate. The compounds were printed on a 384-well white plate using a randomization feature (n = 1).

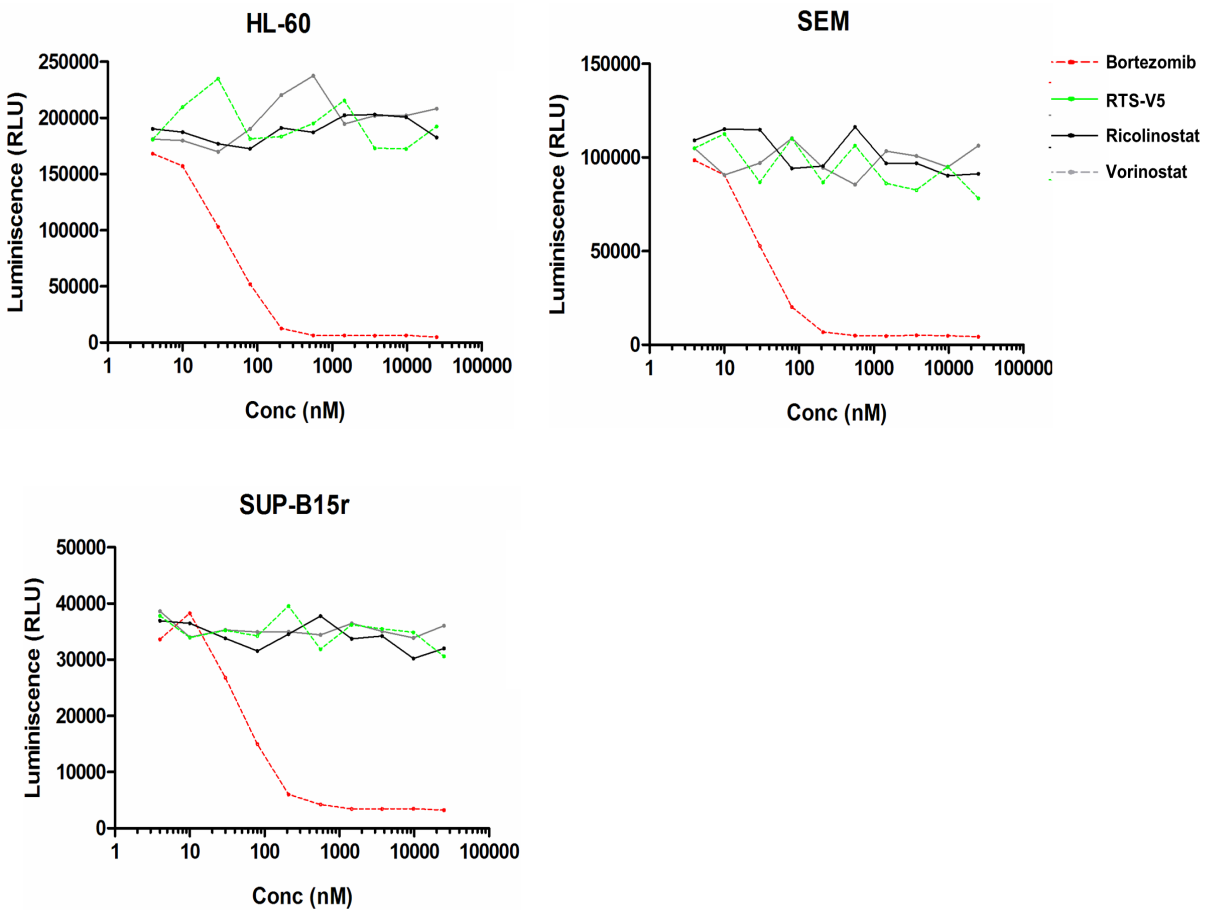

Figure S1b. Proteasome inhibition assay (Caspase-like activity). HL-60, SEM, KCL-22r, and SUP-B15r cells were treated for 2 h with bortezomib, vorinostat, ricolinostat, and RTS-V5 at concentrations ranging from 4 nM-25 µM. The proteasomal activity was measured after 2 h using a Cell-Based Proteasome-Glo Chymotrypsin-Like assay by taking Z-nLPnLD-aminoluciferin (Z-norleucine-proline-norleucine-aspartate-aminoluciferin) as a substrate. The compounds were printed on a 384-well white plate using a randomization feature (n = 1).

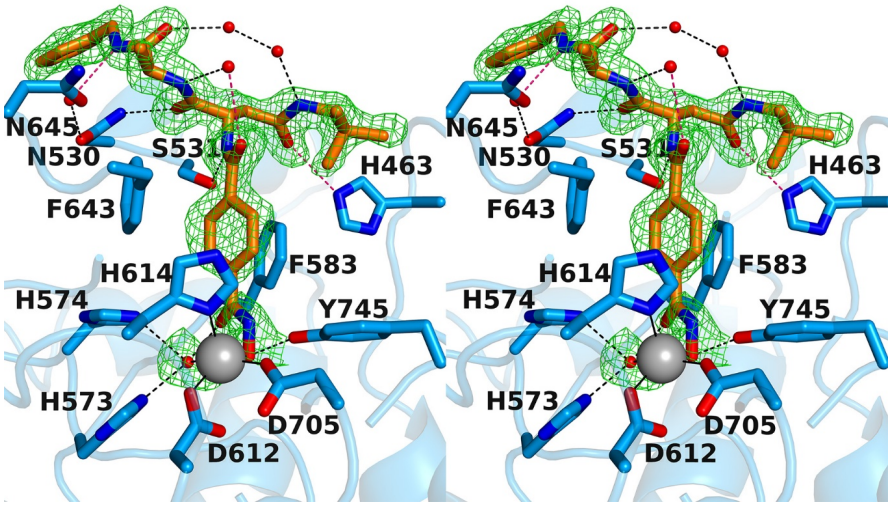

Figure S2. Polder omit map of RTS-V5 bound to monomer B of HDAC6 (contoured at 3.0 σ). Atoms are color-coded as follows: C = orange (RTS-V5) or light blue (protein), N = blue, O = red, Zn^{2+} = gray sphere, solvent = red spheres. Metal coordination and hydrogen bond interactions are indicated by solid and dashed black lines, respectively. Also indicated are interactions that are slightly too long for hydrogen bonding, with nonhydrogen atom separations of 3.3 Å (dashed red lines). In monomer B, the benzyl-L-alanyl moiety adopts an alternative conformation from that observed in monomer A. This results in a different array of hydrogen bonds in comparison with those observed in monomer A (Figure S3). The amide carbonyl group to which this moiety is attached accepts a hydrogen bond from N530 (O---N distance = 2.8 Å). The side chain of N530 also forms a hydrogen bond with a water molecule that is within hydrogen bonding distance from the benzamide NH group. Notably, N530 is specific to zebrafish HDAC6 and appears as an aspartate residue in human HDAC6. Thus, interactions observed for N530 in zebrafish HDAC6 will differ from those that would be expected for binding to human HDAC6. Specifically, an aspartate in place of N530 could not be a hydrogen bond donor to RTS-V5. Consequently, the binding mode observed in monomer B would be disfavored, and the binding mode observed in monomer A would be favored, in the RTS-V5 complex with human HDAC6.

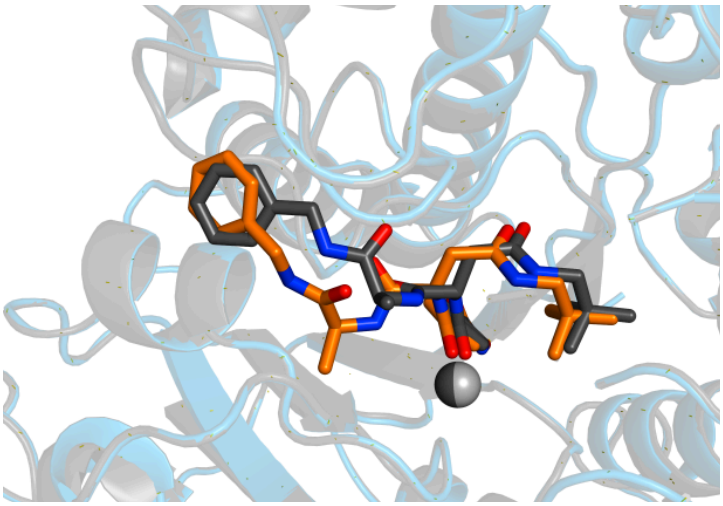

Figure S3. Superposition of monomers A and B of the HDAC6–RTS-V5 complex. Although there are no major structural changes between the two monomers, the benzyl-L-alanyl moiety of RTS-V5 adopts alternative conformations in each monomer. RTS-V5 is color-coded as follows: C = black (monomer A) or orange (monomer B), N = blue, O = red, Zn^{2+} = gray sphere.

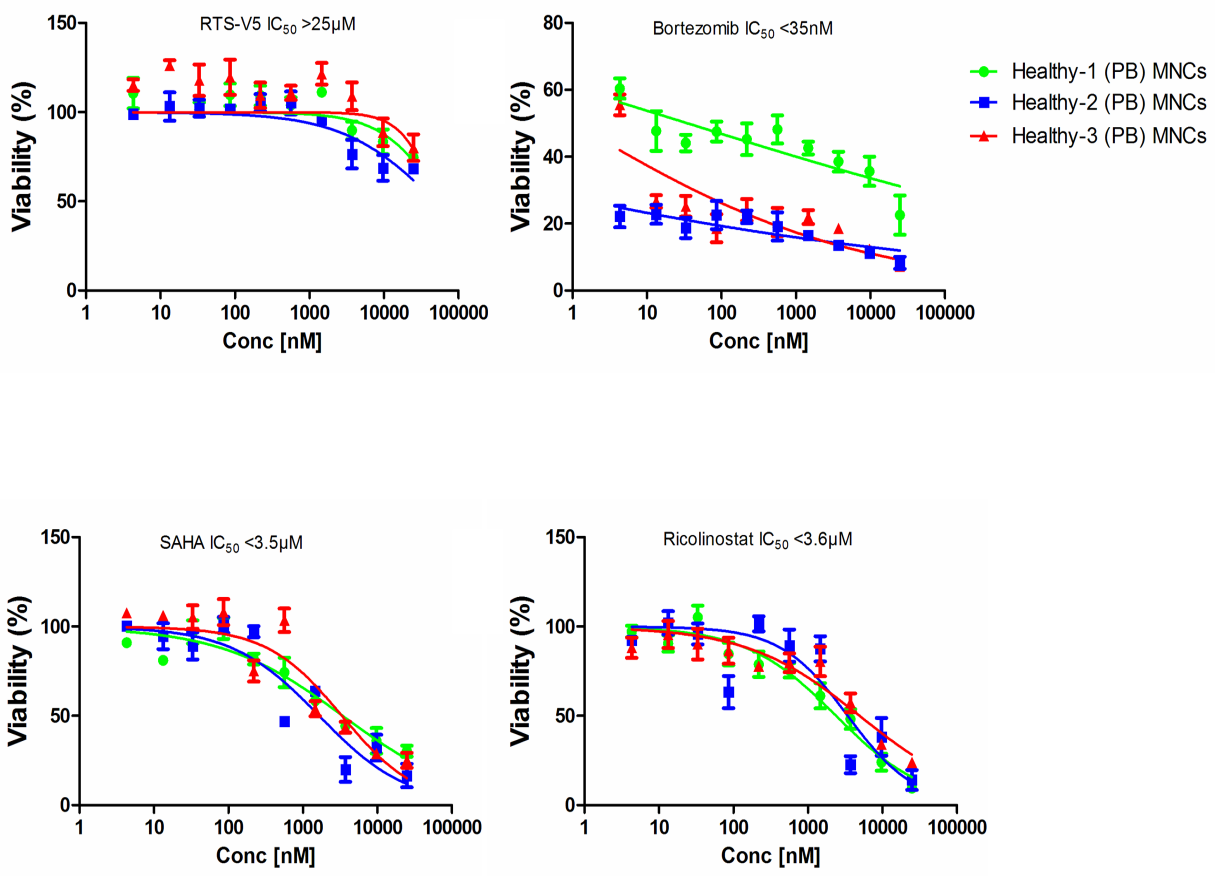

Figure S4. Toxicity against mononuclear cells from peripheral blood. 3 healthy individuals-derived mononuclear cells (MNCs) from peripheral blood (PB) were treated with RTS-V5, bortezomib, ricolinostat, and vorinostat for 72 h at concentrations ranging from 4 nM-25 µM. The average IC_{50} (n = 3) was determined by Celltitre-Glo assay.

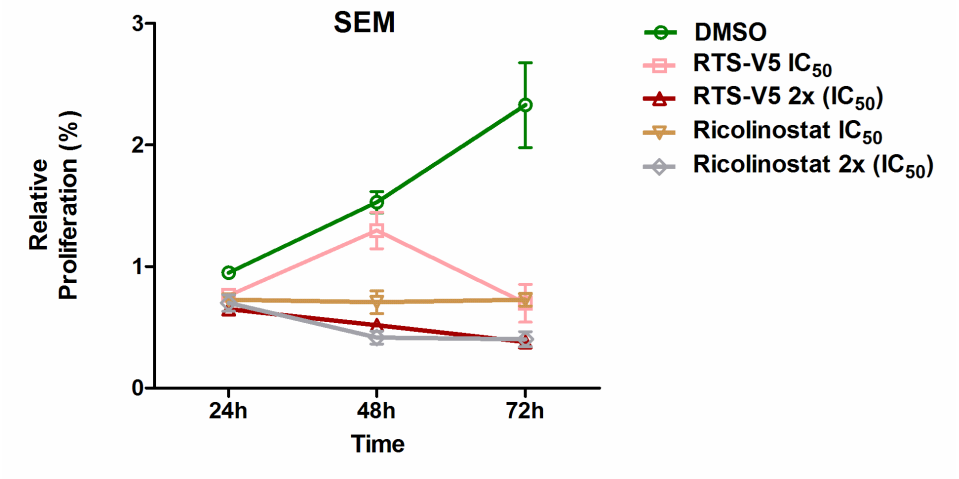

Cell line	Incubation time	DMSO (x10^{6}cells/ml)	RTS-V5 IC_{50} (x10^{6}cells/ml)	RTS-V5 2x (IC_{50}) (x10^{6}cells/ml)	Ricolinostat IC_{50} (x10^{6}cells/ml)	Ricolinostat 2x (IC_{50}) (x10^{6}cells/ml)
SEM	24 h	0.94 ± 0.02	0.76 ± 0.04*	0.64 ± 0.02**	0.72 ± 0.02*	0.70 ± 0.06*
	48 h	1.52 ± 0.08	1.29 ± 0.15	0.51 ± 0.02*	0.70 ± 0.09*	0.41 ± 0.05**
	72 h	2.32 ± 0.34	0.69 ± 0.15*	0.38 ± 0.02*	0.72 ± 0.05*	0.40 ± 0.06*

Figure S5. Proliferation assay. SEM were treated with RTS-V5 and ricolinostat at IC_{50} and two times (2x) the IC_{50} concentrations and later the viable cells were counted after 24 h, 48 h, and 72 h (n = 3). Significance analyses of normally distributed data with variance similar between groups used paired, two-tailed Student's t-test. * $p < 0.05$, ** $p < 0.005$, *** $p < 0.001$.

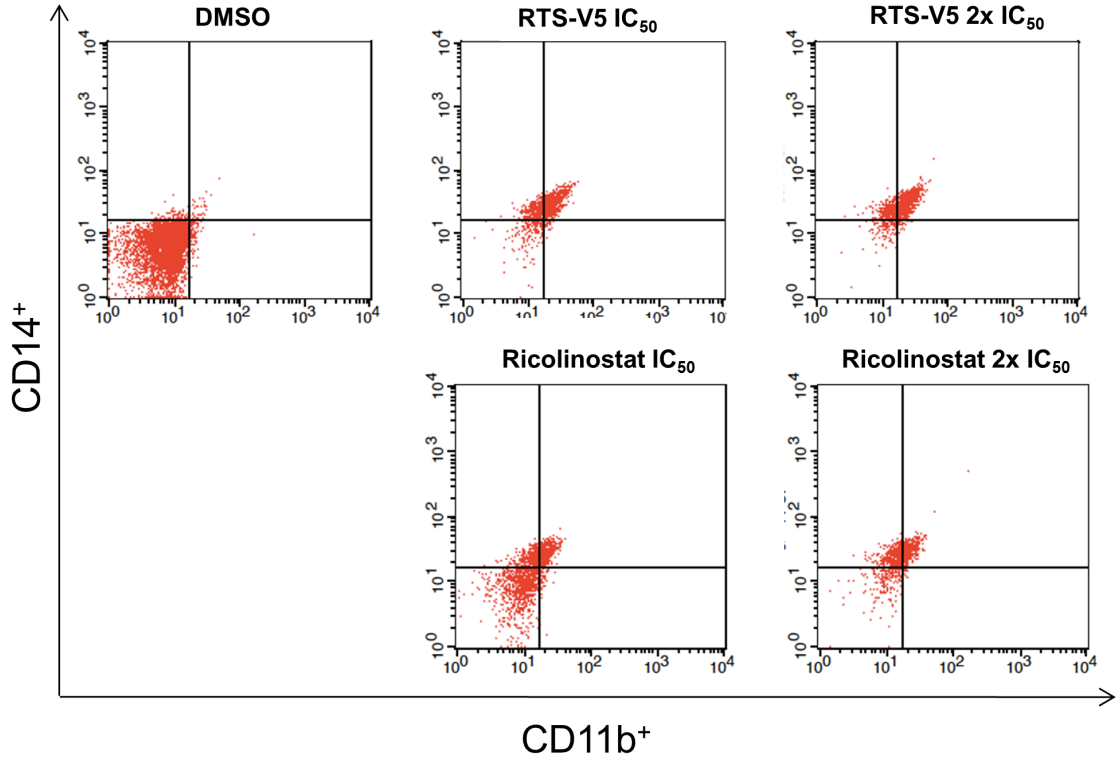

Cell line	Treatment	CD11b$^+$ (% of cells)	CD14$^+$ (% of cells)	(CD11b$^+$ CD14$^+$) (% of cells)
SEM	DMSO	1.84	2.19	0.60
	RTS-V5 IC_{50}	55.61	83.31	53.63
	RTS-V5 2x (IC_{50})	58.83	88.41	57.26
	Ricolinostat IC_{50}	19.25	42.81	17.10
	Ricolinostat 2x (IC_{50})	34.82	79.35	33.49

Figure S6. Differentiation analysis (in liquid medium). SEM were treated with RTS-V5 and ricolinostat at IC_{50} and two times (2x) the IC_{50} concentrations for 72 h and were subjected to FACS after staining with CD11b and CD14 antibodies respectively. Diagrams show bivariate FACS analysis of CD11b vs. CD14 and in the below panel the table representing the percentages cells in different compartments.

Table S1. Data collection and refinement statistics for the HDAC6–RTS-V5 complex.

Data Collection	
Space group	$C222_1$
Unit cell Dimensions	
a, b, c (Å)	48.3, 128.4, 260.5
α, β, γ (°)	90.0, 90.0, 90.0
Resolution (Å)	64.20–1.90 (1.94–1.90)[a]
R_{merge}[b]	0.350 (1.51)[a]
R_{pim}[c]	0.124 (0.592)[a]
$CC_{1/2}$[d]	0.977 (0.656)[a]
Redundancy	8.8 (7.8)[a]
Completeness (%)	100.0 (100.0)[a]
I/σ	7.0 (2.9)[a]
Refinement	
Resolution (Å)	45.22–1.90 (1.97–1.90)[a]
No. reflections	64448 (6332)[a]
R_{work}/R_{free}[e]	0.151/0.188 (0.200/0.254)[a]
No. atoms[f]	
Protein	5579
Ligand	118
Solvent	522
Average B factors (Å^2)	
Protein	11
Ligand	18
Solvent	18
R.m.s. deviations	
Bond Lengths (Å)	0.006
Bond Angles (°)	0.8
Ramachandran Plot (%)[g]	
Favored	97.0
Allowed	3.0
Outliers	0.00

[a]Values in parentheses refer to the highest-resolution shell indicated. [b]$R_{merge} = \sum_{hkl}\sum_i|I_{i,hkl} - \langle I\rangle_{hkl}|/\sum_{hkl}\sum_i I_{i,hkl}$, where $\langle I\rangle_{hkl}$ is the average intensity calculated for reflection *hkl* from replicate measurements. [c]$R_{p.i.m.} = (\sum_{hkl}(1/(N-1))^{1/2}\sum_i|I_{i,hkl} - \langle I\rangle_{hkl}|)/\sum_{hkl}\sum_i I_{i,hkl}$, where $\langle I\rangle_{hkl}$ is the average intensity calculated for reflection *hkl* from replicate measurements and N is the number of reflections [d]Pearson correlation coefficient between random half-datasets. [e]$R_{work} = \sum||F_o| - |F_c||/\sum|F_o|$ for reflections contained in the working set. $|F_o|$ and $|F_c|$ are the observed and calculated structure factor amplitudes, respectively. R_{free} is calculated using the same expression for reflections contained in the test set held aside during refinement. [f]Per asymmetric unit. [g]Calculated with PROCHECK.

Table S2. X-ray data collection and refinement statistics for the yCP: RTS-V5 complex.

	yCP: **RTS-V5**
Crystal parameters	
Space group	$P2_1$
Cell constants	a = 137.1 Å b = 300.8 Å c = 145.1 Å β = 113.5 °
CP / AU[a]	1
Data collection	
Beam line	X06SA, SLS
Wavelength (Å)	1.0
Resolution range (Å)[b]	50-2.5 (2.6-2.5)
No. observations	1160973
No. unique reflections[c]	362822
Completeness (%)[b]	97.9 (98.6)
R_{merge} (%)[b, d]	5.1 (56.8)
I/σ (I)[b]	14.7 (2.5)
Refinement (REFMAC5)	
Resolution range (Å)	15-2.5
No. refl. working set	343137
No. refl. test set	18059
No. non hydrogen	50266
No. of ligand atoms	76
Solvent (H_2O, Mg^{2+}, Cl^-)	866
R_{work}/R_{free} (%)[e]	18.7 / 21.7
r.m.s.d. bond (Å) / (°)[f]	0.007 / 1.1
Average B-factor (Å^2)	69.4
Ramachandran Plot (%)[g]	97.9/ 1.9 / 0.2
PDB accession code	6H39

[a] Asymmetric unit

[b] The values in parentheses for resolution range, completeness, R_{merge} and I/σ (I) correspond to the highest resolution shell

[c] Data reduction was carried out with XDS and from a single crystal. Friedel pairs were treated as identical reflections

[d] $R_{merge}(I) = \Sigma_{hkl}\Sigma_j \mid I(hkl)_j - \langle I(hkl)\rangle \mid / \Sigma_{hkl}\,\Sigma_j\, I(hkl)_j$, where $I(hkl)_j$ is the j^{th} measurement of the intensity of reflection hkl and $\langle I(hkl)\rangle$ is the average intensity

[e] $R = \Sigma_{hkl} \mid |F_{obs}| - |F_{calc}| \mid / \Sigma_{hkl} |F_{obs}|$, where R_{free} is calculated without a sigma cut off for a randomly chosen 5% of reflections, which were not used for structure refinement, and R_{work} is calculated for the remaining reflections

[f] Deviations from ideal bond lengths/angles

[g] Number of residues in favored region / allowed region / outlier region

2. Chemistry

Preparation of 4-((benzyloxy)carbamoyl)benzoic acid

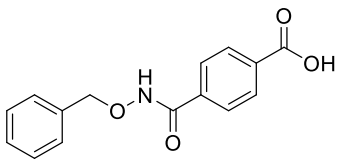

Methyl 4-((benzyloxy)carbamoyl)benzoate (800 mg, 2.8 mmol, 1 eq) was dissolved in 20 mL THF. Lithium hydroxide monohydrate (470 mg, 11.2 mmol, 4 eq) was added and the resulting solution was stirred at room temperature for 24 h. After completion of the reaction, the mixture was acidified using 1 M HCl (pH ≈ 1) and extracted with ethyl acetate (3 x 20 mL). The combined organics were dried over sodium sulfate and the solvent was removed under reduced pressure. 4-((benzyloxy)carbamoyl)benzoic acid was crystallized from *n*-hexane and ethyl acetate.

4-((benzyloxy)carbamoyl)benzoic acid. White solid; 73% yield; mp. 227–230 °C; ^{1}H-NMR (600 MHz, DMSO-d_6): δ 13.24 (bs, 1H, OH), 11.94 (s, 1H, 1H), 8.05 – 7.98 (m, 2H, arom. H), 7.86 – 7.80 (m, 2H, arom. H), 7.50 – 7.34 (m, 5H, arom. H), 4.94 (s, 2H, OCH_2) ppm; ^{13}C-NMR (151 MHz, DMSO-d_6): δ 166.7, 163.6, 136.1, 135.8, 133.4, 129.4, 129.0, 128.3, 127.4, 77.1 ppm; HRMS (m/z): M^- calcd. for $C_{15}H_{12}NO_4$, 270.0772; found, 270.0767.

3. X-ray crystallography

X-ray crystal structure determination of HDAC6 in complex with RTS-V5. HDAC6 catalytic domain 2 (CD2, residues 440–798) from *Danio rerio* (zebrafish) was recombinantly expressed using the MBP-TEV-z6CD2-Pet28a(+) vector[1] and purified as described.[1,2] Briefly, zebrafish HDAC6 CD2 (henceforth, simply "HDAC6") was expressed in *Escherichia coli* BL21 (DE3) cells in 2xYT media with 50 mg/L kanamycin. Cells were grown at 37° C until OD_{600} reached 1.0, after which the temperature was decreased to 18 °C for an additional 18 h. Cells were supplemented with 200 μM $ZnSO_4$ and induced with 75 μM isopropyl β-L-1-thiogalactopyranoside. Cells were sonicated in buffer A [50 mM K_2HPO_4 (pH 8.0), 300 mM NaCl, 1 mM tris(2-carboxyethyl)phosphine (TCEP), 5% glycerol] and centrifuged at 15,000 *g* for 1 h at 4° C, after which the supernatant was purified using an amylose column (New England BioLabs); protein was eluted using 10 mM maltose in buffer A. Protein fractions were dialyzed overnight in buffer A plus 10 mg/mL TEV protease to cleave the MBP tag. The digested protein sample was then applied to a Ni-NTA column (Qiagen) in Buffer A and protein was eluted in a 0–300 mM imidazole gradient. HDAC6-containing fractions were was loaded onto a HiLoad superdex 200 column in buffer B [50 mM HEPES (pH 7.5), 100 mM KCl, 1 mM TCEP, 5% glycerol] and concentrated to approximately 10 mg/mL. Protein was flash-cooled in liquid nitrogen and stored at -80 ˚C prior to use.

The HDAC6–RTS-V5 complex was crystallized by the vapor diffusion method at 4° C by equilibrating a 0.70 μL sitting drop consisting of 0.35 μL protein solution [10 mg/mL HDAC6, 50 mM 4-(2-hydroxyethyl)-1-piperazineethanesulfonic acid (HEPES) (pH 7.5), 2.0 mM RTS-V5, 100 mM KCl, 1 mM TCEP, 5% glycerol] and 0.35 μL precipitant solution [0.2 M LiCl, 20% w/v polyethylene glycol 3,350] against a reservoir of 100 μL precipitant solution. Thick plate-like crystals appeared within 3 days. Crystals were harvested and soaked in crystallization buffer augmented with 20% ethylene glycol as a cryoprotectant prior to flash cooling in liquid nitrogen.

X-ray diffraction data were collected at AMX beamline 17-ID-1 at the National Synchrotron Light Source II (NSLS-II), Brookhaven National Laboratory. Data were indexed and integrated using iMOSFLM[3] and scaled using Aimless in the CCP4 program suite.[4] While R_{merge} values were rather high for these data, the corresponding $CC_{1/2}$ values were well within accepted ranges; this phenomenon is often observed for datasets with high redundancies. The crystal structure of the HDAC6–RTS-V5 complex was solved by molecular replacement using the atomic coordinates of unliganded HDAC6 (PDB 5EEM) as a search probe for rotation and

translation function calculations using the program Phaser.[5] Crystallographic structure refinement was achieved using Phenix,[6] and the graphics software Coot[7] was used to inspect and adjust the model of the enzyme-inhibitor complex between refinement runs. Inhibitor and solvent molecules were added in the later stages of refinement. Spurious electron density peaks were occasionally observed that could not be satisfactorily modeled by solvent components, and such peaks were left uninterpreted. The overall quality of the final protein model was evaluated using MolProbity and PROCHECK.[8,9] Final refinement statistics are recorded in Supplementary Table 1. Polder omit electron density maps were calculated as described.[10] Final refined coordinates and structure factor amplitudes for the final model have been deposited in the Protein Data Bank (www.rcsb.org) with accession code 6CW8.

Protein crystallography of the yeast 20S proteasome in complex with RTS-V5. Crystals of the 20S yeast proteasome (yCP) were grown in hanging drops at 20 °C as described.[11,12] The protein concentration used for crystallization was 40 mg/ml in 10 mM tris(hydroxymethyl)aminomethane (TRIS)-HCl (pH 7.5). The drops were composed of 2 µl of protein and 2 µl of the reservoir solution, containing 30 mM magnesium acetate, 100 mM morpholino-ethane-sulphonic acid (MES)-NaOH (pH 7.2) and 10 % 2-methyl-2,4-pentanediol (MPD). Crystals were incubated overnight with the linear decarboxylated peptide RTS-V5. In the following, crystals were soaked in a cryoprotecting buffer (30 % MPD, 20 mM magnesium acetate, 100 mM MES-NaOH pH 6.9) and vitrified in a stream of liquid nitrogen gas at 100 K. Diffraction data for the yCP:RTS-V5 complex structure were collected to 2.5 Å using synchrotron radiation with λ= 1.0 Å at the beamline X06SA, Swiss Light Source (SLS), Villigen, Switzerland. X-ray intensities were evaluated by the XDS program package[13] including data reduction. Conventional crystallographic rigid body, positional and temperature factor refinements were carried out with REFMAC5 using coordinates of the yeast 20S proteasome structure (PDB ID 5CZ4) as starting model.[14] For model building the programs MAIN[15] and COOT[16] were used, respectively.

Protein Data Bank accession code. Coordinates have been deposited in the RCSB Protein Data Bank under the accession code 6H39.

4. ^{1}H- and ^{13}C-NMR spectra

Compound **3**: ^{1}H-NMR (400 MHz, DMSO-d_6)

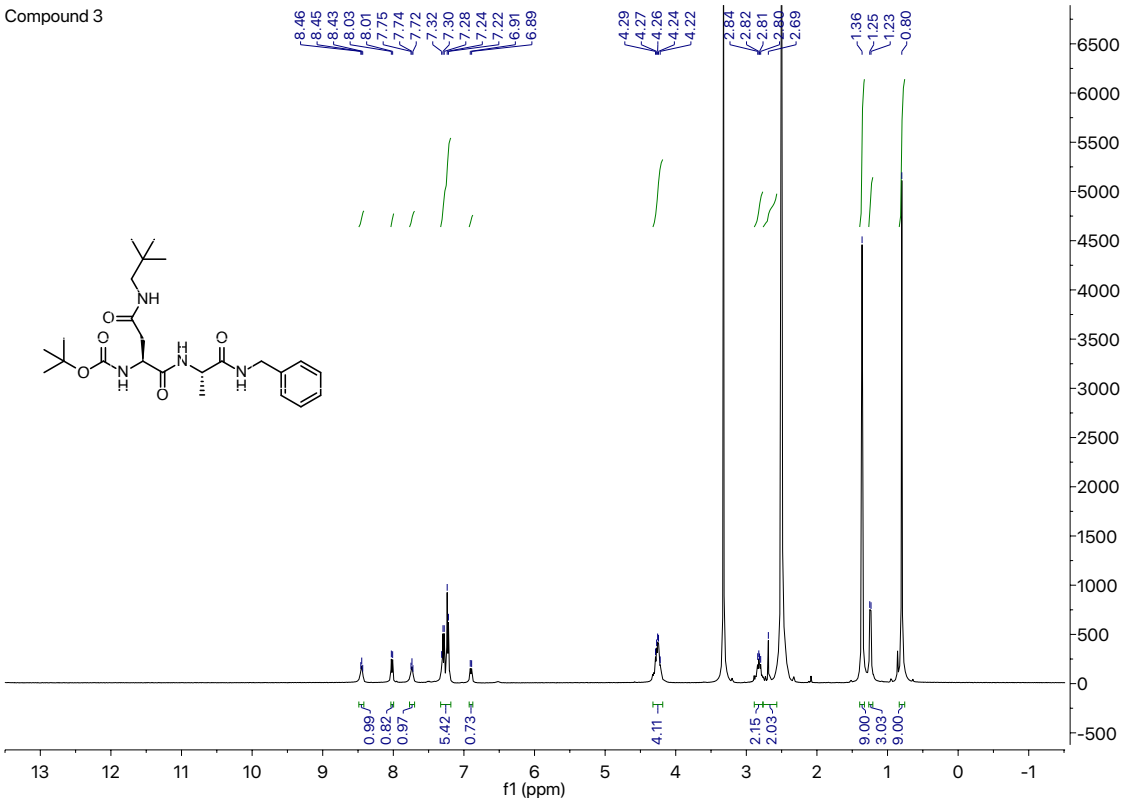

Compound **3**: ^{13}C-NMR (101 MHz, DMSO-d_6)

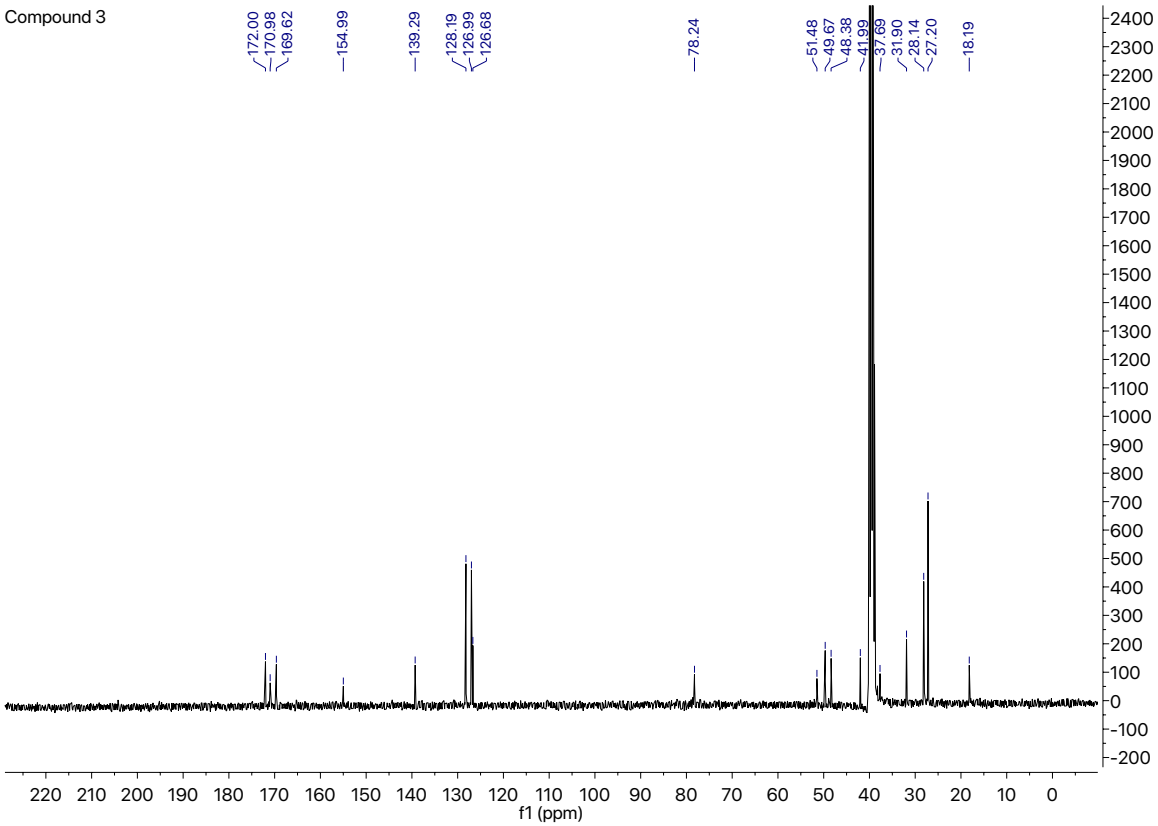

Compound 4-((benzyloxy)carbamoyl)benzoic acid: ^{1}H-NMR (600 MHz, DMSO-d_6)

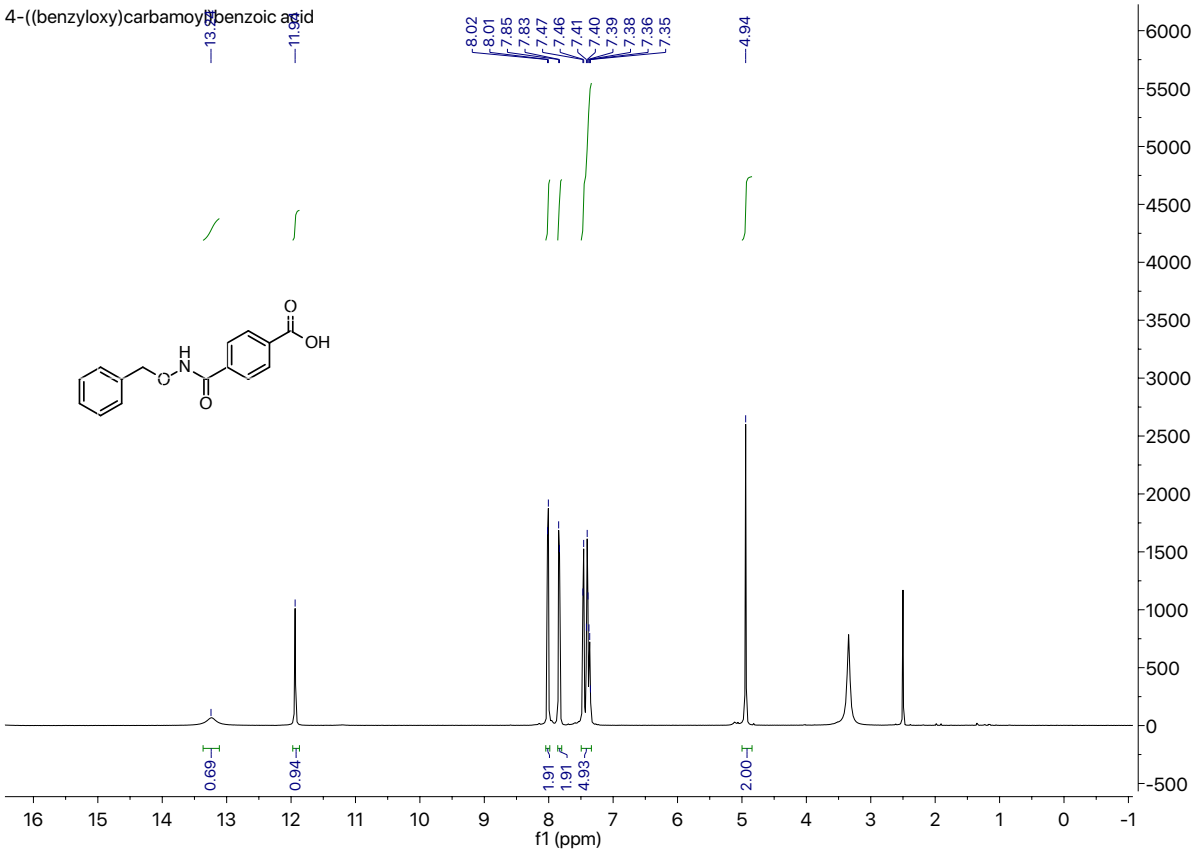

Compound 4-((benzyloxy)carbamoyl)benzoic acid: ^{13}C-NMR (151 MHz, DMSO-d_6)

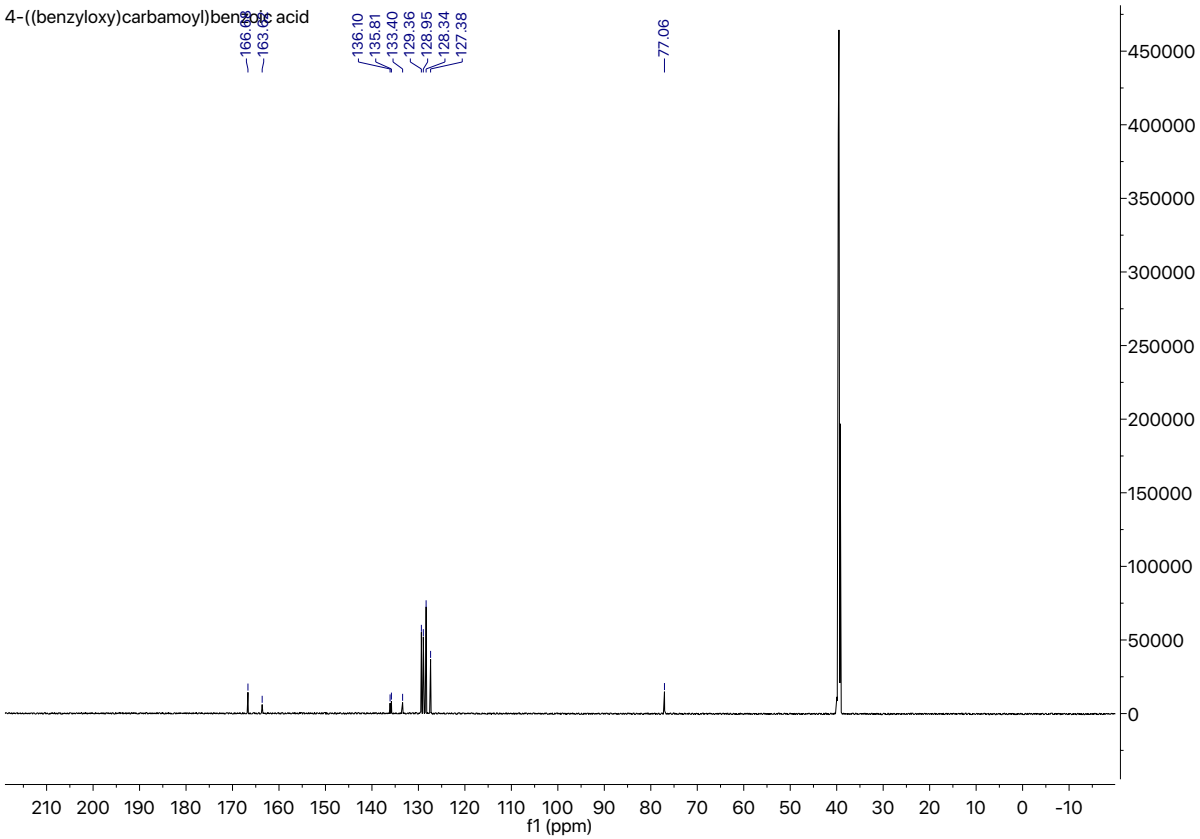

Compound **4**: ^{1}H-NMR (400 MHz, DMSO-d_6)

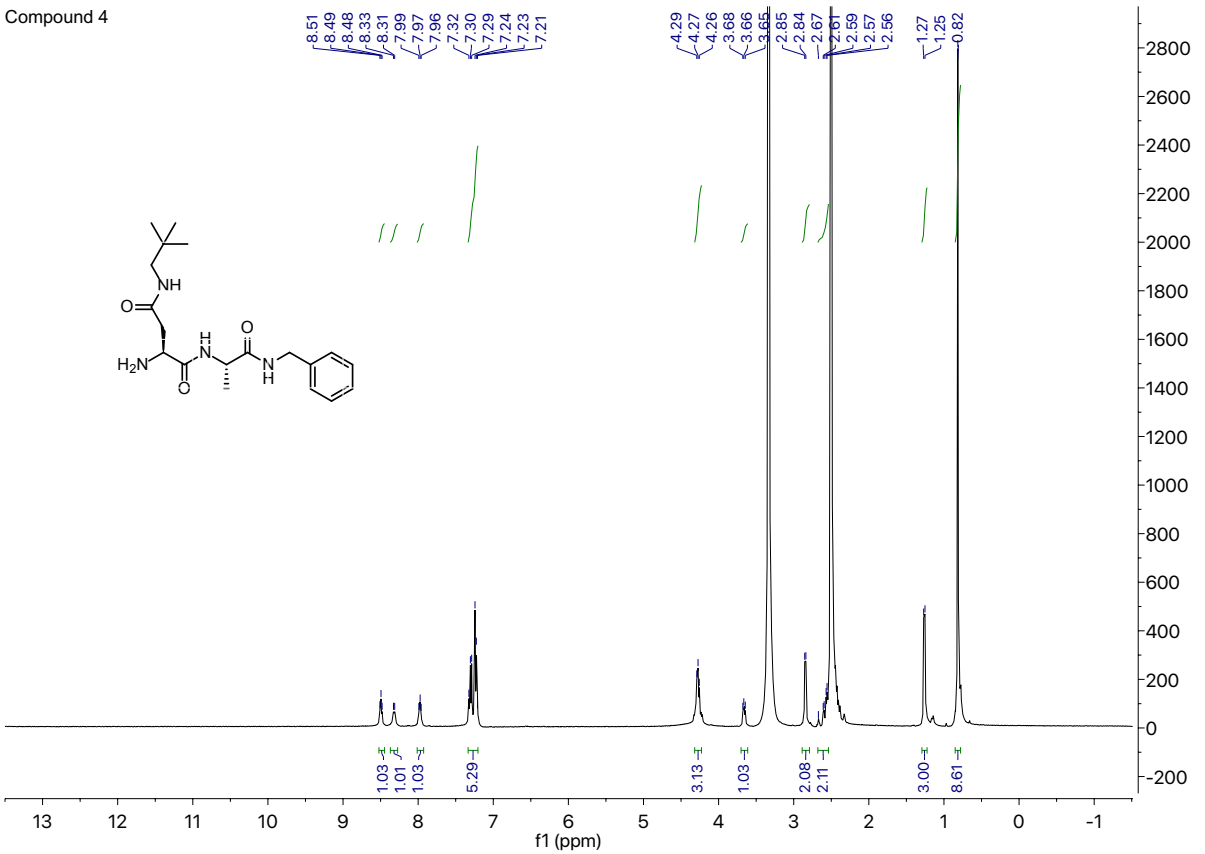

Compound **4**: ^{13}C-NMR (75 MHz, DMSO-d_6)

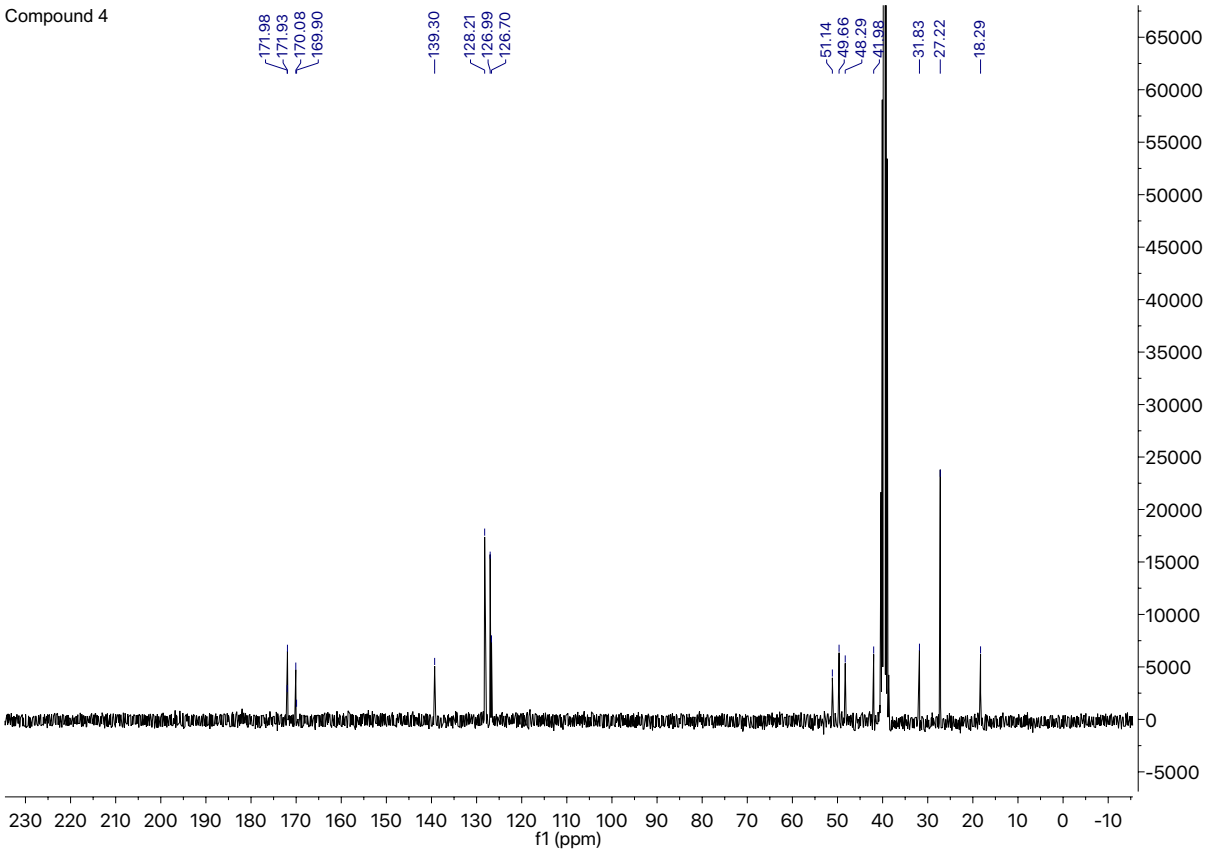

Compound **5**: ^{1}H-NMR (400 MHz, DMSO-d_6)

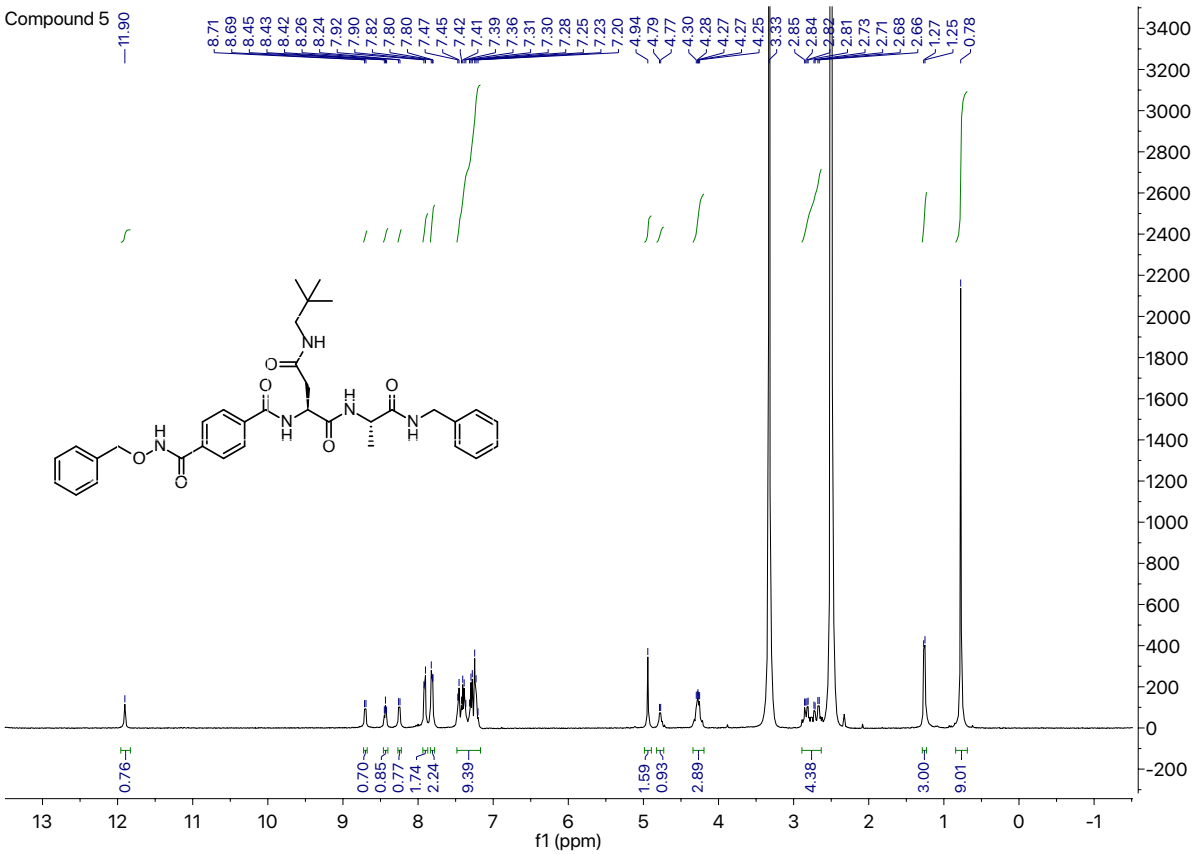

Compound **5**: ^{13}C-NMR (101 MHz, DMSO-d_6)

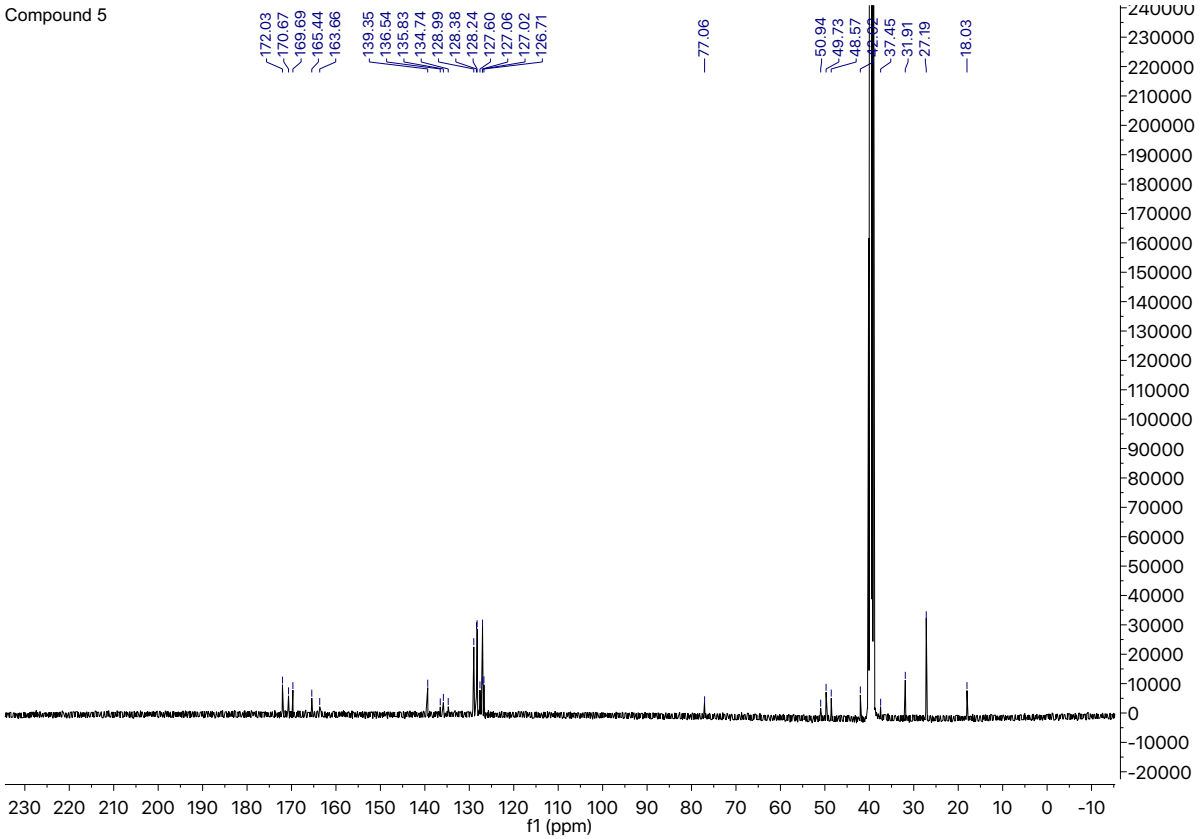

Compound **RTS-V5**: ^{1}H-NMR (500 MHz, DMSO-d_6)

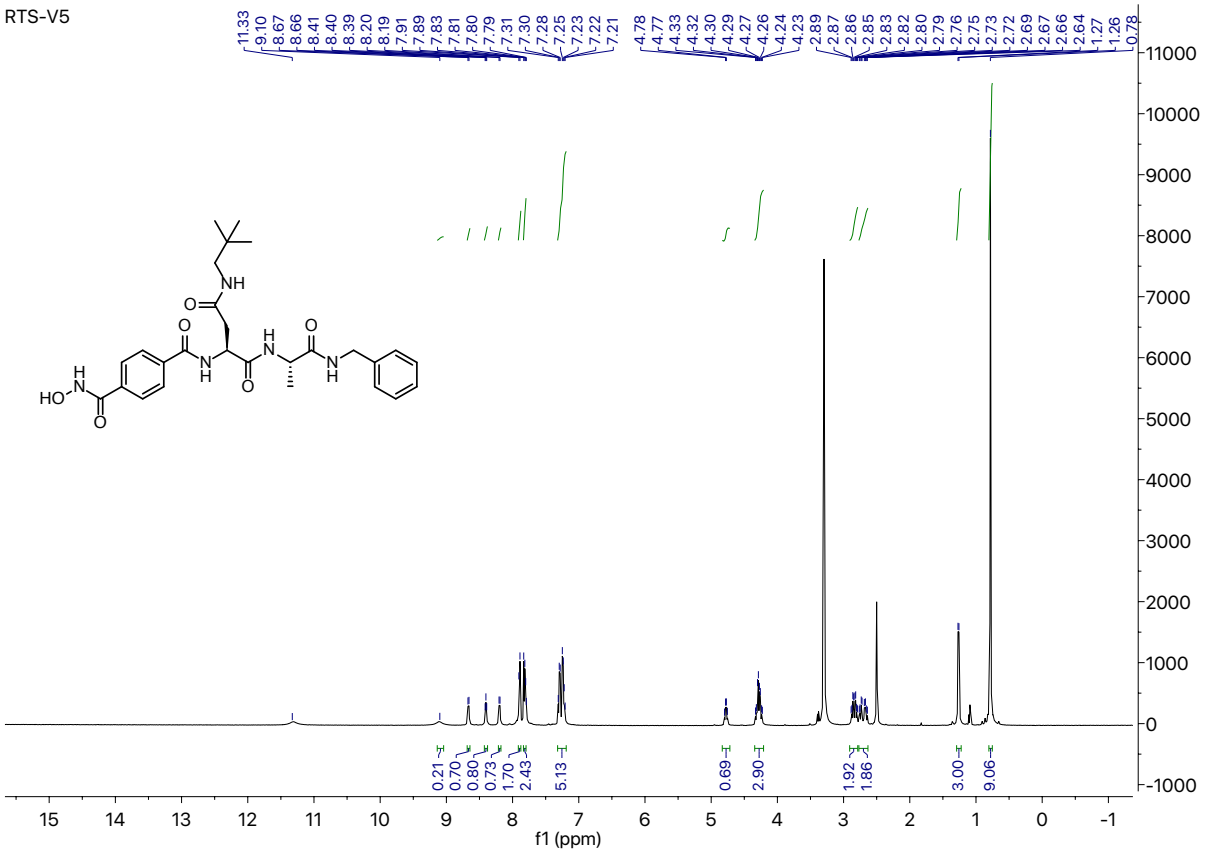

Compound **RTS-V5**: ^{13}C-NMR (126 MHz, DMSO-d_6)

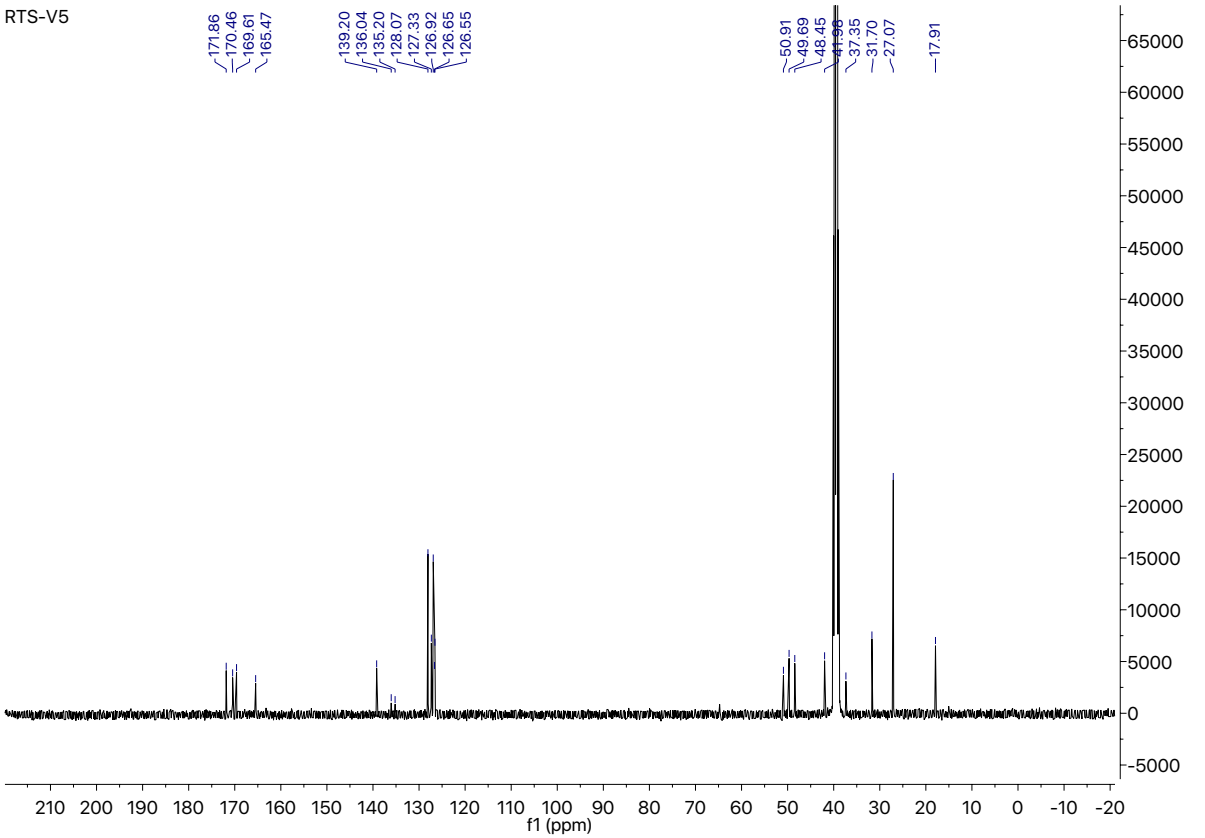

HPLC chromatogram of **RTS-V5**

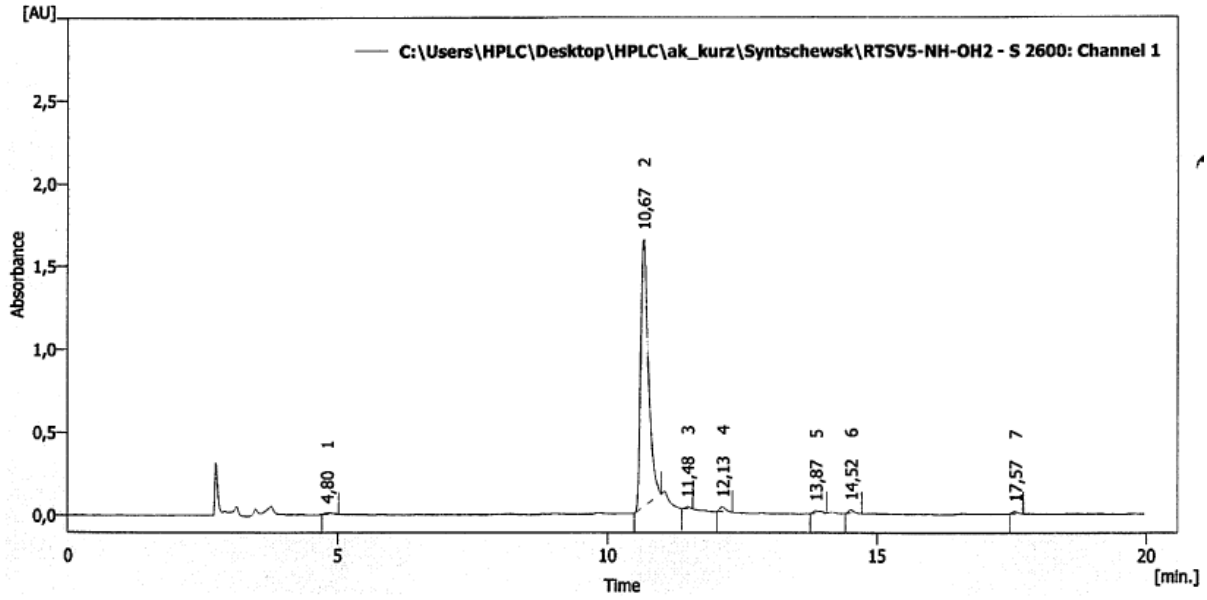

Result Table (Uncal - C:\Users\HPLC\Desktop\HPLC\ak_kurz\Syntschewsk\RTSV5-NH-OH2 - S 2600: Channel 1)

	Reten. Time [min]	Start Time [min]	End Time [min]	Area [mAU.s]	Height [mAU]	Area [%]	Height [%]	Compound Name
1	4,800	4,717	5,017	110,315	11,625	0,6	0,7	
2	10,667	10,500	11,000	16221,908	1613,173	95,0	93,6	
3	11,483	11,383	11,583	76,036	12,696	0,4	0,7	
4	12,133	12,033	12,317	227,982	30,503	1,3	1,8	
5	13,867	13,767	14,067	166,955	16,485	1,0	1,0	
6	14,517	14,417	14,717	169,914	22,841	1,0	1,3	
7	17,567	17,467	17,717	105,470	15,320	0,6	0,9	
	Total			17078,581	1722,644	100,0	100,0	

5. References

1. Hai, Y, Christianson, D. W. Histone deacetylase 6 structure and molecular basis of catalysis and inhibition. *Nat. Chem. Biol*. **12**, 741–747 (2016).

2. Porter, N. J., Mahendran, A., Breslow, R. and Christianson, D.W. Unusual zinc-binding mode of HDAC6-selective hydroxamate inhibitors. *Proc. Natl. Acad. Sci. U. S. A*. **114**, 13459–13464 (2017).

3. Battye, T. G. G., Kontogiannis, L., Johnson, O., Powell, H. R., Leslie, A. G. W. iMOSFLM: a new graphical interface for diffraction-image processing with MOSFLM. *Acta Crystallogr. D Biol. Crystallogr.* **67**, 271–281 (2011).

4. Winn, M. D., Ballard, C. C., Cowtan, K. D., Dodson, E. J., Emsley, P., Evans, P. R., Keegan, R. M., Krissinel, E. B., Leslie, A. G. W., McCoy, A., McNicholas, S. J., Murshudov, G. N., Pannu, N. S., Potterton, E. A., Powell, H. R., Read, R. J., Vagin, A., Wilson, K. S. Overview of the CCP4 suite and current developments. *Acta Crystallogr. D Biol. Crystallogr*. **67**, 235–242 (2011).

5. McCoy, A. J., Grosse-Kunstleve, R. W., Adams, P. D., Winn, M. D., Storoni, L. C., Read, R. J. *Phaser* crystallographic software. *J. Appl. Cryst***. 40**, 658–674 (2007).

6. Adams, P. D., Afonine, P. V., Bunkóczi, G., Chen, V. B., Davis, I. W., Echols, N., Headd, J. J., Hung, L., Kapral, G. J., Grosse-Kunstleve, R. W., McCoy, A. J., Moriarty, N. W., Oeffner, R., Read, R. J., Richardson, D. C., Richardson, J. S., Terwilliger, T. C., Zwart, P. H. PHENIX: a comprehensive Python-based system for macromolecular structure solution. *Acta Crystallogr. D Biol. Crystallogr.* **66**, 213–221 (2010).

7. Emsley, P., Lohkamp, B., Scott, W.G., Cowtan, K. Features and development of Coot. *Acta Crystallogr. D Biol. Crystallogr*. **66**, 486–501 (2010).

8. Chen, V. B., Arendall, W. B., III, Headd, J. J., Keedy, D. A., Immormino, R. M., Kapral, G. J., Murray, L. W., Richardson, J. S., Richardson, D. C. MolProbity: all-atom structure validation for macromolecular crystallography. *Acta Crystallogr. D Biol. Crystallogr*. **66**, 12–21 (2010).

9. Laskowski, R.A., MacArthur, M.W., Moss, D.S., Thornton, J.M. PROCHECK: A program to check the stereochemical quality of protein structures. *J Appl. Cryst.* **26**, 283–291 (1993).

10. Liebschner, D., Afonine, P. V., Moriarty, N. W., Poon, B. K., Sobolev, O. V., Terwilliger, T. C., Adams, P. D. Polder maps: improving OMIT maps by excluding bulk solvent. *Acta Crystallogr. D Biol. Crystallogr.* **73**, 148–157 (2017).

11. Gallastegui N., Groll M. Analysing properties of proteasome inhibitors using kinetic and X-ray crystallographic studies. *Methods Mol. Biol.* **832**, 373–390 (2012).

12. Groll M., Huber R. Purification, crystallization, and X-ray analysis of the yeast 20S proteasome. *Methods Enzymol.* **398**, 329–336 (2005).

13. Kabsch, W. XDS. *Acta Crystallogr. D Biol. Crystallogr*. **66**, 125–132 (2010).

14. Huber, E. M., Heinemeyer, W., Li, X., Arendt, C. S., Hochstrasser, M., Groll, M. A unified mechanism for proteolysis and autocatalytic activation in the 20S proteasome. *Nat Commun.* **7**, 10900 (2016).

15. Turk, D. MAIN software for density averaging, model building, structure refinement and validation. *Acta Crystallogr. D Biol. Crystallogr*. **69**, 1342–1357 (2013).

16. Emsley P., Cowtan K. Coot: model-building tools for molecular graphics. *Acta Crystallogr. D Biol. Crystallogr*. **60**, 2126–2132 (2004).